Direct Evidence of Dirac Signature in Bilayer Germanene Islands on Cu(111)

Zhihui Qin, Jinbo Pan, Shuangzan Lu, Yan Shao, Yeliang Wang, Shixuan Du, Hong-Jun Gao, and Gengyu Cao**

"Graphene-like" 2D materials composed of elements other than carbon, that is, silicene and germanene, have been predicted to host a variety of exceptional physical properties,[1–5] holding exciting promises for novel electronic devices.[6,7] In particular, the spin–orbit coupling in germanene is rather strong due to the large atomic number of germanium. Germanene with puckered geometry has been predicted to have a spin–orbit band gap of 23.9 meV (corresponding to 277 K) at the Dirac point (DP) in the interior of germanene, resulting in experimentally detectable quantum spin Hall effect.[2] To date germanene has been realized by epitaxial growth of germanium on a variety of metallic surfaces, such as Pt(111),[8] Au(111),[9] and Al(111),[10,11] and has been directly observed at the termination of 3D Ge_2Pt islands on Ge(110).[12,13] However, the hybridization of the electronic states near the Fermi level with the electronic states of the underlying metal might either modify or destroy the Dirac state of the 2D adlayers.[14–19] Of late, the intense research into this promising new material has generally focused on experimental realization of germanene with the Dirac signature.

Theoretically, the Dirac state in 2D germanene adlayer exhibits when germanene interacts with the substrate via a weak van der Waals (vdW)-type interaction,[15,20–22] as has been experimentally demonstrated for germanene islands on graphite and molybdenum disulfide,[23,24] for instance. However, the weak adlayer–substrate interactions are unfavorable for stabilizing the buckled geometry, which typically requires a metallic support as the bottom substrate. Another way to mitigate the influence of the metal substrate is to insert a buffer layer decoupling the germanene adlayer from the substrate,[16] as has been experimentally demonstrated for germanene overgrowth on *h*-AlN/Ag(111),[25] and on hexagonal boron nitride (*h*-BN) theoretically predicted in a recent review paper.[26] Unfortunately, no direct STM image with real atomic resolution was provided in the former case.

Prof. Z. Qin, Dr. S. Lu, Prof. G. Cao
State Key Laboratory of Magnetic Resonance and Atomic and Molecular Physics
Wuhan Institute of Physics and Mathematics
Chinese Academy of Sciences
Wuhan 430071, P. R. China
E-mail: gycao@wipm.ac.cn

Dr. J. Pan, Y. Shao, Prof. Y. Wang, Prof. S. Du, Prof. H.-J. Gao
Institute of Physics and University of Chinese Academy of Sciences
Chinese Academy of Sciences
Beijing 100190, P. R. China
E-mail: sxdu@iphy.ac.cn

DOI: 10.1002/adma.201606046

We report the growth of bilayer germanene on Cu(111) demonstrating for the first time the presence of a nearly linear energy dispersion in the vicinity of the Fermi energy. Cu(111) was adopted as the growth template because of its hexagonal symmetry without surface reconstruction, matching lattice, and relatively weaker interfacial interaction with adsorbates than other metals, and so on (see details in the Supporting Information). Atomic structures and electronic characteristics of the obtained germanene have been well explored by LT-STM/S in combination with first-principles DFT calculations. For monoatomic-layer (ML) germanene, the STS spectrum loses features of the Dirac state, albeit a honeycomb arrangement of 1×1 germanene lattice is clearly revealed. On the other hand, we rationalize the structure of biatomic-layer (BL) germanene as Bernal stacking. It is fascinatingly that a V-shaped differential conductivity curve is obtained on the top germanene layer, with a nonzero electronic state minimum. Charge density difference calculation presents compelling evidence of the absence of charge transfer between the top germanene layer and the copper substrate. Moreover, electron localization function (ELF) calculations reveal 2D continuity of the BL germanene. Combining experimental observations with DFT calculations, we conclude that the top germanene layer is efficiently decoupled from the copper substrate by the bottom germanene layer acting as a buffer layer, thus the Dirac state exhibits.

Figure 1a shows an STM image of a germanium island. On the island, the honeycomb structure with real atomic resolution is clearly visualized. The nearest neighbor distance in the honeycomb lattice is measured as ≈2.54 Å (Figure S1, Supporting Information), a little longer than the theoretically predicted bond length of 2.38 Å in a germanene layer.[27] The difference is likely due to a partial relief of the misfit strain of the system. Notably, the perimeters of the germanene island have zigzag orientations. And inhomogeneous perturbation of the relevant electronic states by the underlying metallic substrate is observed to be superimposed on the honeycomb structure. A relaxed ML germanene structure optimized by first-principles calculations is schematically shown in Figure 1b. The relaxed 1×1 germanene structure is closely commensurate with the Cu(111) lattice and nicely matches the observed honeycomb lattice, giving strong evidence that the islands are ML germanene, wherein germanium atoms tend to situate in the hollow sites of Cu(111) and lie perfectly flat on the substrate after relaxation.

Figure 2a shows other kinds of nanometer-sized germanium islands formed on Cu(111) with almost twice the apparent height (Figure S1, Supporting Information) of the monolayer. Note that the edges of these islands coincide with the dense Cu rows, along the close-packed direction of Cu⟨1-10⟩ deduced

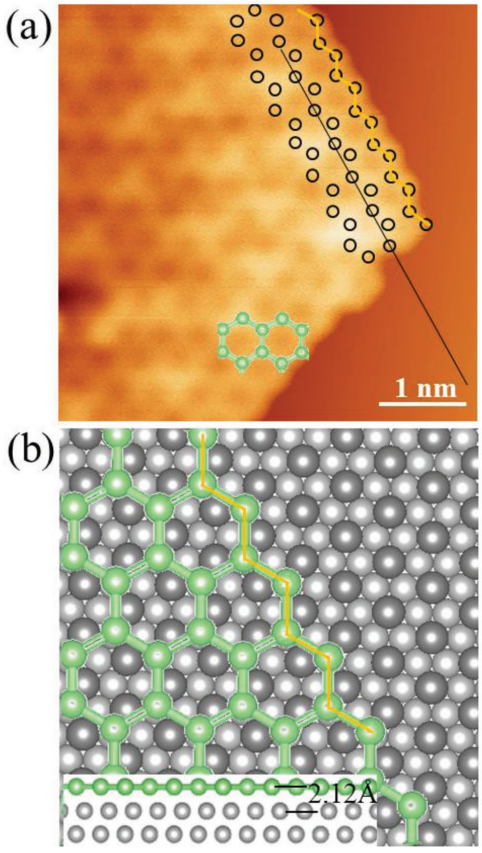

Figure 1. Monoatomic-layer germanene on Cu(111). a) Topographic STM image ($V = -0.10$ V, $I = 0.03$ nA). The honeycomb structure (atoms visible at all six vertices of the hexagon) is seen over the entire sheet. A ball-and-stick model showing the honeycomb geometry is superimposed on the image as a guide for the eyes. b) Top view of the relaxed atomic model of the 1 × 1 germanene/Cu(111) configuration. The perimeter is also indicated with a zigzag geometry. (Inset) Side view of the configuration shows the planarity of germanium atoms with respect to the underlying Cu lattice.

from the atomic resolution of Cu(111) (Figure 2b). This suggests that, during epitaxy, germanium atoms prefer to nucleate and align with the lattice of the underlying Cu(111). In contrast to the honeycomb lattice of ML germanene (Figure 1a), by further close inspection of the islands a triangular structure with an edge length of ≈4.38 Å is observed (Figure 2c). The rotation angle between the triangular lattice and Cu⟨1-10⟩ is 30°. Considering the commensuration with Cu(111), we tentatively define the obtained germanium islands as a ($\sqrt{3} \times \sqrt{3}$) R30° superstructure with respect to Cu(111).

The origin of the triangular structure can be well elucidated by the first-principles calculations, in which the ($\sqrt{3} \times \sqrt{3}$) R30° superstructure was built by pure germanium and substituted Cu impurities (Figure S2, Supporting Information). The corresponding formation enthalpies were calculated and compared from an energetic point of view. The Bernal-stacked BL structure (Figure 2d), wherein half the atoms in the top layer sit on top of the empty centers of hexagons in the bottom germanium layer, has the minimum energy. And the relaxed lattice constant is calculated to be ≈4.32 Å, quite close to the experimental value (4.38 Å), and the interlayer distance between the two sheets is calculated as ≈2.70 Å. Based on these we conclude that the germanium islands are Bernal-stacked BL germanene islands. In addition, due to the misfit strain of the system, the observed and calculated lattice constants are a little larger than the hexagonal lattice constant (3.97–4.02 Å) of the honeycomb structure expected for a freestanding germanene layer.[2,27,28] Also, the extent of the buckling is calculated as ≈0.61 Å. Indeed, the observation of a triangular sublattice is a reflection of the buckling. STM simulation further supports this conclusion. As shown in Figure 2e buckled-up Ge atoms in the upper layer dominate the simulated STM image, in excellent agreement with the STM observations (Figure 2c), verifying that the model in Figure 2d fundamentally resembles what we observed in our experiments. The relaxed ($\sqrt{3} \times \sqrt{3}$) R30° model and the simulated STM image present a clear picture of the germanium arrangements in the BL germanene. The topmost germanium atoms (red balls in Figure 2d) correspond to the bright protrusions in the STM image.

Bias dependence of differential conductance, a quantity proportional to the local DOS,[29] was recorded on the lattices of ML (red curve in **Figure 3**) and BL (black curve) germanene, respectively, to clarify the electronic structure of our germanene. Because the dI/dV spectrum is sensitive to the termination of STM tip, good condition and stability of the tip was verified by checking the standard spectrum (inset of Figure 3) of the pristine Cu(111) before acquiring each dI/dV curve. Consistent dI/dV spectra were acquired on ML and BL germanene, respectively. For the sake of comparison, the recorded curves were put into one panel. In contrast to the red curve, in the vicinity of the Fermi level, the black curve is linear energy dispersion and shows well-defined V-shaped differential conductivity, which could be attributed to a 2D Dirac system.[12,24] To rationalize this, we performed projected DOS (Figure S3, Supporting Information) calculations by first-principles DFT (see details in the Supporting Information). It is important to notice that a well-defined V-shaped density of states in the vicinity of the Fermi level can only form in Bernal stacking BL germanene, not so in the twisted BL germanene. If the top germanene layer has a twist angle θ ($\theta = 0°$ for Bernal stacking BL germanene) with respect to the underlying germanene layer, the Dirac cone splits into two separate Dirac cones, two Van Hove singularities develop, similar to the case of twisted bilayer graphene,[30] and destroy the nice V-shape of the density of states. Significantly, the DP is offset by 30 meV above the Fermi level (identified with zero bias) indicating unintentional doping with hole carriers. Moreover, the tunneling conductance at the DP has a nonzero value (a finite DOS).

With these in mind, we performed charge density calculations to evaluate the coupling between the BL germanene and the substrate, in particular to understand the phenomenon of a finite DOS at the DP. The differential charge density shown in **Figure 4**a,b provides information about the electron redistribution between BL germanene and Cu(111). Very clearly, the electron redistribution mainly involves half the germanium atoms in the bottom layer and no charge transfers between the top germanene layer and the substrate. Copper atoms act as electron acceptors and gain electrons from these germanium atoms, leading to hole carrier doping in germanene, thus the offset of

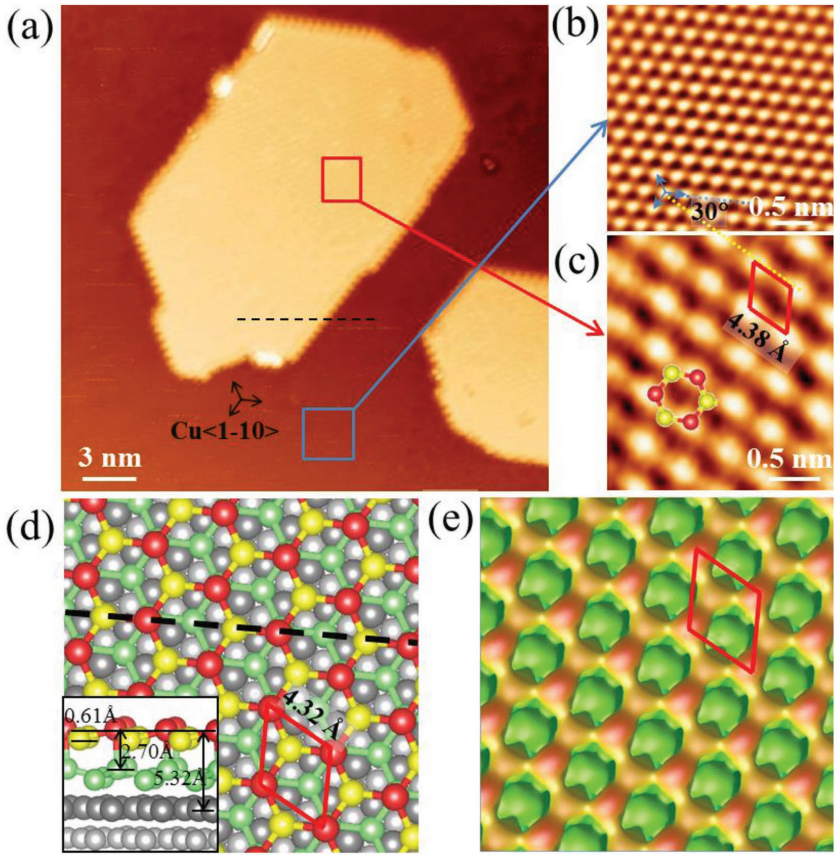

Figure 2. Biatomic-layer germanene on Cu(111). a) Unoccupied-states STM image ($V = 0.07$ V, $I = 0.07$ nA), showing well-shaped 2D germanium nanosheets. The perimeters of the germanene sheets run parallel to the close-packed direction Cu⟨1-10⟩, deduced from b) the atomic resolution STM image of the pristine Cu(111) (blue contour). c) Zoomed-in STM image ($V = 0.06$ V, $I = 0.07$ nA) of a germanium adlayer (red contour), revealing the periodicity of the germanene superstructure (4.38 Å). The angle between the blue and yellow dotted lines is about 30°. d) Schematic illustrating (top view) the relaxed atomic model of the ($\sqrt{3} \times \sqrt{3}$) R30° BL germanene/Cu(111) configuration. (Inset) Side view of the configuration reveals a corrugation of around 0.61 Å in the adlayer and the interlayer distance between the two germanium layers of 2.70 Å. One unit cell is indicated as a red rhombus. e) Simulated STM image with the features fitting very well with the experimental observations.

the DP. Moreover, charge density difference analysis further confirms that the top layer is electronically decoupled from the copper substrate by the bottom germanene buffer layer. This does not, however, imply that these germanene islands possess all the intriguing properties theoretically expected for freely suspended germanene. The interlayer coupling interferes. The nature of the interlayer bonding was further ascertained by the following ELF calculation.[31,32]

ELF reveals the charge localization between individual atoms, allowing us to directly appraise the interaction between atoms. Figure 4c shows the top view of the overall ELF within the germanene layer with an ELF value of 0.50, confirming the continuity of the BL germanene. Germanium atoms are shown to be well bonded to each other. In order to distinctly identify the bonding characteristics within each germanium pair, the ELFs along the cross sections of each Ge—Ge pair are displayed in Figure 4d. The ELF values are shown by color scheme, where the red signifies highly localized electrons and the blue represents the electrons with almost no localization. Obviously, electrons are localized to a large degree at the Ge—Ge pairs (the ELF values are in the range of 0.65–0.84), providing strong evidence that a covalent interaction exists between the members of each Ge—Ge pair, both within a germanene layer and between the germanene layers. Covalent interaction within the interior of germanene layer demonstrates the 2D continuity of BL germanene. Moreover, the interlayer interaction leads to the buckling of every layer, and produces additional states at the DP, giving rise to a finite tunneling conductance there. For comparison, the ELF value between the germanium atom and its nearest Cu atom is also calculated to be only 0.24, much smaller than the ELF values of any of the germanium pairs. ELF values of less than 0.50 correspond to an absence of pairing between electrons. Therefore, it can be concluded that the interaction between germanium and the underlying copper is mainly of an electrostatic origin.

In conclusion, Bernal-stacked germanene BL nanosheet with ($\sqrt{3} \times \sqrt{3}$) R30° superstructure in terms of the underlying Cu(111) lattice has been structurally characterized by STM and is in accordance with the DFT optimized structure. Due to electronically decoupling of the bottom germanene layer, the bilayer germanene makes possible the appearance of the Dirac signature expected of freestanding germanene. Moreover, the calculated ELF unequivocally certifies that continuous 2D BL germanene was achieved, and the interlayer coupling produces additional states at the DP leading to a finite DOS there. Copper-supported BL germanene with a buckled honeycomb structure and the Dirac state might be a functional material for miniaturized germanene-based nanoelectronics directly fabricated on copper without a delamination transfer process.

Experimental Section

Sample Preparation: Experiments were performed in an ultrahigh vacuum (UHV) system with a base pressure about 3×10^{-10} mbar. The Cu(111) substrate was cleaned by several cycles of Ar^+ sputtering (500 eV, 15 min) and subsequent annealing (≈850 K, 10 min) until it yielded clean surface terraces in STM images. High purity Ge (Alfa Aesar Puratronic 99.9999+%) was evaporated from a thermally heated crucible onto Cu(111) kept at room temperature, with the Ge flux estimated to be ≈0.03 ML min^{-1}. After deposition, the sample was heated up to 450 K (480 K) in 20 s (30 s) and kept at 450 K (480 K) with a very small fluctuation of about 2 K for 20 min (10 min), respectively. The samples were annealed at temperatures less than 500 K to prevent formation of Ge—Cu surface alloy. Then LT-STM was employed to image the surface at liquid nitrogen temperature in the constant-current mode with bias voltage V applied to the sample. STM images were processed using

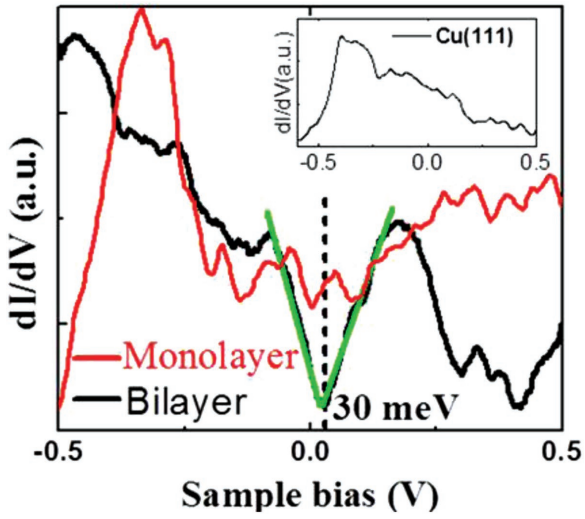

Figure 3. Bias dependence of the tunneling conductance dI/dV, obtained on the surface of ML (red) and BL (black) germanene, respectively. (Inset) STS spectrum taken on the bare Cu(111) repeatedly verifying the condition of the tip. Set points: Sample bias $V = 1.0$ V and tunneling current $I = 0.1$ nA.

WSxM.[33] The tunneling conductance dI/dV was measured by extracting lock-in amplifier derivation of the I/V signal with 777 Hz bias voltage modulation.

Computation: The DFT-based first-principles calculations were performed using the Vienna ab initio simulation package (VASP).[34,35] The projector augmented wave (PAW) potentials were used to describe the core electrons, and local density approximation (LDA) was used for exchange and correlation.[36] The periodic slab models included four layers of Cu, one or two layers of germanium, and a vacuum layer of 15 Å. All atoms were fully relaxed, except for the bottom two substrate layers, until the net force on every atom was less than 0.01 eV Å^{-1}.

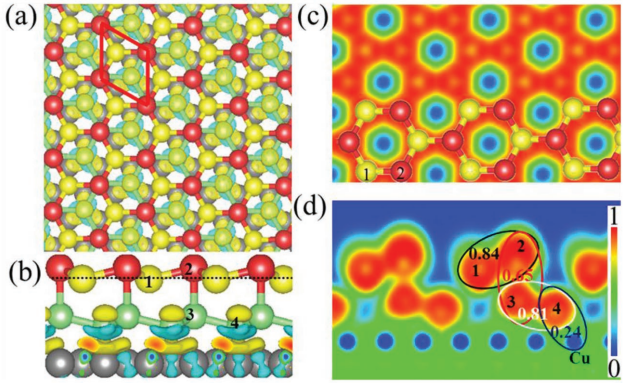

Figure 4. Electron redistribution and localization of BL germanene on Cu (111). a) Top view and b) side view of calculated differential charge density of the ($\sqrt{3} \times \sqrt{3}$) R30° germanene/Cu(111). Yellow and blue represent obtaining and losing electrons, respectively. Isosurfaces value: 0.005 e Å^{-3}. c) Top view of the overall electron localization function (ELF) of the relaxed model, cut from the dotted line in (b) with an ELF value of 0.5, showing continuity of the germanene layer. The color scale is the same as that in (d). d) The ELFs of the cross sections between germanium pairs, showing the covalent interaction existing between each pair of germanium atoms. The ELF value of the cross section between one germanium atom and its nearest Cu atom is in the range of the green-blue region (about 0.24), indicating an electrostatic interaction. The color scale is shown on the right.

The energy cutoff of the plane-wave basis sets was 400 eV, and the K-points sampling was 11 × 11 × 1, generated automatically with the origin at the Γ-point. The differential charge density was calculated by $\Delta\rho = \rho_{tot} - \rho_{Ge} - \rho_{sub}$, where ρ_{tot}, ρ_{Ge}, and ρ_{sub} are the total charge density of Ge adlayer on Cu (111) substrate, charge density of pure Ge adlayer, and pure Cu (111) substrate, respectively. Structures were visualized by the VESTA software.[37]

Supporting Information

Supporting Information is available from the Wiley Online Library or from the author.

Acknowledgements

Z.Q. and J.P. contributed equally to this work. The authors gratefully acknowledge financial support from the National Key Basic Research Program of China (No. 2013CBA01600), the National Key Research and Development Projects of China (No. 2016YFA0202300), the National Natural Science Foundation of China (Nos. 11574350, 61390501, and 51325204).

Received: November 9, 2016
Revised: December 18, 2016
Published online: January 30, 2017

[1] S.-C. Wu, G. Shan, B. Yan, *Phys. Rev. Lett.* **2014**, *113*, 256401.
[2] C.-C. Liu, W. Feng, Y. Yao, *Phys. Rev. Lett.* **2011**, *107*, 076802.
[3] L. Seixas, J. E. Padilha, A. Fazzio, *Phys. Rev. B* **2014**, *89*, 195403.
[4] T. Amlaki, M. Bokdam, P. J. Kelly, *Phys. Rev. Lett.* **2016**, *116*, 256805.
[5] N. J. Roome, J. D. Carey, *ACS Appl. Mater. Interfaces* **2014**, *6*, 7743.
[6] Z. Ni, Q. Liu, K. Tang, J. Zheng, J. Zhou, R. Qin, Z. Gao, D. Yu, J. Lu, *Nano Lett.* **2012**, *12*, 113.
[7] N. D. Drummond, V. Zólyomi, V. I. Fal'ko, *Phys. Rev. B* **2012**, *85*, 075423.
[8] L. Li, S.-Z. Lu, J. Pan, Z. Qin, Y.-Q. Wang, Y. Wang, G. Cao, S. Du, H.-J. Gao, *Adv. Mater.* **2014**, *26*, 4820.
[9] M. E. Dávila, L. Xian, S. Cahangirov, A. Rubio, G. Le Lay, *New J. Phys.* **2014**, *16*, 095002.
[10] M. Derivaz, D. Dentel, R. Stephan, M.-C. Hanf, A. Mehdaoui, P. Sonnet, C. Pirri, *Nano Lett.* **2015**, *15*, 2510.
[11] Y. Fukaya, I. Matsuda, B. Feng, I. Mochizuki, T. Hyodo, S. Shamoto, *2D Mater.* **2016**, *3*, 035019.
[12] L. Zhang, P. Bampoulis, A. van Houselt, H. J. W. Zandvliet, *Appl. Phys. Lett.* **2015**, *107*, 111605.
[13] P. Bampoulis, L. Zhang, A. Safaei, R. van Gastel, B. Poelsema, H. J. W. Zandvliet, *J. Phys. Condens. Matter* **2014**, *26*, 442001.
[14] C.-L. Lin, R. Arafune, K. Kawahara, M. Kanno, N. Tsukahara, E. Minamitani, Y. Kim, M. Kawai, N. Takagi, *Phys. Rev. Lett.* **2013**, *110*, 076801.
[15] Z. Guo, S. Furuya, J. Iwata, A. Oshiyama, *Phys. Rev. B* **2013**, *87*, 235435.
[16] L. Li, M. Zhao, *Phys. Chem. Chem. Phys.* **2013**, *15*, 16853.
[17] Y. Wang, J. Li, J. Xiong, Y. Pan, M. Ye, Y. Guo, H. Zhang, R. Quhe, J. Lu, *Phys. Chem. Chem. Phys.* **2016**, *18*, 19451.
[18] S. K. Mahatha, P. Moras, V. Bellini, P. M. Sheverdyaeva, C. Struzzi, L. Petaccia, C. Carbone, *Phys. Rev. B* **2014**, *89*, 201416.
[19] M. X. Chen, Z. Zhong, M. Weinert, *Phys. Rev. B* **2016**, *94*, 075409.
[20] Y. Cai, C.-P. Chuu, C. M. Wei, M. Y. Chou, *Phys. Rev. B* **2013**, *88*, 245408.
[21] T. P. Kaloni, U. Schwingenschlögl, *J. Appl. Phys.* **2013**, *114*, 184307.

[22] X. Li, S. Wu, S. Zhou, Z. Zhu, *Nano Res. Lett.* **2014**, *9*, 110.
[23] L. Persichetti, F. Jardali, H. Vach, A. Sgarlata, I. Berbezier, M. De Crescenzi, A. Balzarotti, *J. Phys. Chem. Lett.* **2016**, *7*, 3246.
[24] L. Zhang, P. Bampoulis, A. N. Rudenko, Q. Yao, A. van Houselt, B. Poelsema, M. I. Katsnelson, H. J. W. Zandvliet, *Phys. Rev. Lett.* **2016**, *116*, 256804.
[25] F. d¢Acapito, S. Torrengo, E. Xenogiannopoulou, P Tsipas, J. M. Velasco, D. Tsoutsou, A. Dimoulas, *J. Phys.: Condens. Matter* **2016**, *28*, 045002.
[26] A. Acun, L. Zhang, P. Bampoulis, M. Farmanbar, A. van Houselt, A. N. Rudenko, M. Lingenfelder, G. Brocks, B. Poelsema, M. I. Katsnelson, H. J. W. Zandvliet, *J. Phys. Condens. Matter* **2015**, *27*, 443002.
[27] S. Cahangirov, M. Topsakal, E. Aktürk, H. Şahin, S. Ciraci, *Phys. Rev. Lett.* **2009**, *102*, 236804.
[28] C.-C. Liu, H. Jiang, Y. Yao, *Phys. Rev. B* **2011**, *84*, 195430.
[29] J. Tersoff, D. R. Hamann, *Phys. Rev. B* **1985**, *31*, 805.
[30] G. Li, A. Luican, J. M. B. L. dos Santos, A. H. C. Neto, A. Reina, J. Kong, E. Y. Andrei, *Nat. Phys.* **2009**, *6*, 109.
[31] A. D. Becke, K. E. Edgecombe, *J. Chem. Phys.* **1990**, *92*, 5397.
[32] A. Savin, O. Jepsen, J. Flad, O. K. Andersen, H. Preuss, H. G. Vonschnering, *Angew. Chem. Int. Ed.* **1992**, *31*, 187.
[33] I. Horcas, R. Fernández, J. M. Gómez-Rodríguez, J. Colchero, J. Gómez-Herrero, A. M. Baro, *Rev. Sci. Instrum.* **2007**, *78*, 013705.
[34] D. Vanderbilt, *Phys. Rev. B* **1990**, *41*, 7872.
[35] G. Kresse, J. Furthmuller, *Phys. Rev. B* **1996**, *54*, 11169.
[36] J. P. Perdew, K. Burke, M. Ernzerhof, *Phys. Rev. Lett.* **1996**, *77*, 3865.
[37] K. Momma, F. Izumi, *J. Appl. Crystallogr.* **2011**, *44*, 1272.